Precision Engineering 38 (2014) 499–505

Contents lists available at ScienceDirect

Precision Engineering

journal homepage: www.elsevier.com/locate/precision

The uncertainty of radius estimation in least-squares sphere-fitting, with an introduction to a new summation based method

Kevin J. Cross, John W. McBride, Joseph J. Lifton*

Electro-Mechanical Research Group, Faculty of Engineering and the Environment, University of Southampton, Highfield SO17 1BJ, UK

ARTICLE INFO

Article history:
Received 12 March 2013
Received in revised form 17 January 2014
Accepted 20 January 2014
Available online 31 January 2014

Keywords:
Least-squares
Sphere-fitting
Design of experiment
Monte Carlo
Uncertainty
Surface metrology
Profilometer

ABSTRACT

This paper considers the sensitivity of three sphere-fitting algorithms to real-world measurement errors. It pays particular attention to nominally spherical surfaces, such as those typically measured by tactile and optical profilometers, addressing the limitations of sensor gauge range and angular tolerance. A recently proposed linear circle-fitting algorithm is extended to a sphere-fitting algorithm and its performance compared to two long standing sphere-fitting algorithms; namely linear and non-linear least-squares. Sources of measurement error in optical profilometers are discussed, and user defined scan parameters are optimised based on the results of a designed experiment. The performance of all three sphere-fitting algorithms are tested on a sphere superimposed with varying degrees of surface irregularities in a Monte Carlo simulation; this study shows that both linear routines display a negative skewness in their radius error distribution. Finally, a method of predicting radius uncertainty is offered that considers the surface residual that remains after sphere-fitting and relates this to the radius uncertainty of the chosen algorithm.

© 2014 Elsevier Inc. All rights reserved.

1. Introduction

The contact lens and other closely linked optical industries have been considering the use of raster-scanning metrology systems for quality assurance since the early 90's [1]. A key objective to quality assurance is for every lens to pass under an instrument to determine its key parameters, for example, radius of curvature, form errors, and lens thickness. In reality, the complex nature of the moulding processes prohibits this approach; it is far simpler to adopt a batch sampling regime. Even with this very limited number of items to measure, the soft, flexible nature of the product, combined with the sources of error inherent in surface metrology instruments makes it difficult and expensive to measure the radius of curvature [2–4].

In previous studies [5,6], sample data has been acquired using the XYRIS 4000, a state-of-the-art surface metrology instrument manufactured by TaiCaan Technologies Ltd. (Southampton, UK). This instrument is custom engineered for applications such as spherical form analysis, adopting a granite gantry to maximise thermal and mechanical stability and using high-precision, 10 nm resolution motion stages coupled with a 10 nm resolution, confocal optical probe. It has been observed that when analysing 3D surface scans there is an error in the estimate of radius of curvature with all sphere-fitting algorithms [6]. In the case of a raster-scanning surface profiler, such as the XYRIS 4000, the probe's gauge range and angular tolerance limit the maximum scan area for nominally spherical objects; this measurement area defines the segment angle of the sphere that is considered by any post-measurement fitting algorithm. Sun et al. [7] considered the impact of the scan area on the algorithms used for calculating the underlying radius of curvature, investigating the performance of non-linear least-squares (NLLS) for small segment angles.

While NLLS has been demonstrated to generally produce the best-fit [6,8,9], it is an iterative algorithm with its solution-time being dependant on both the start estimation and the convergence criteria; furthermore, its speed is also strongly influenced by the size of the data-set, N, following an N^2 relationship. Ultimately, the systematic and random errors present in any real-world measurement system, coupled with the influence of small segment angles, may negate any error reductions from adopting an NLLS algorithm. The aim of this research is to revisit the influence of error sources on the standard least-squares algorithms, while offering a new, alternative algorithm with reduced computational overhead and hence speed benefits.

Section 2 extends a recently proposed linear circle-fitting algorithm to a sphere-fitting algorithm, while Section 3 discusses sources of measurement error in optical profilometers. In Section 4, the impact of three, user-defined scan parameters on the estimated radius are evaluated in a designed experiment. Section 5 compares the performance of the new sphere-fitting algorithm to the existing linear and non-linear least squares algorithms by superimposing

* Corresponding author. Tel.: +44 023 8059 5568; fax: +44 023 8059 301.
E-mail address: J.J.Lifton@soton.ac.uk (J.J. Lifton).

0141-6359/$ – see front matter © 2014 Elsevier Inc. All rights reserved.
http://dx.doi.org/10.1016/j.precisioneng.2014.01.004

varying degrees of Gaussian noise on a simulated, ideal spherical surface in a Monte Carlo simulation. In Section 6, the results of the Monte Carlo simulation are used to predict the uncertainty of the estimated radius for measured data.

2. Least-squares sphere-fitting

The principle of least-squares fitting is well understood, namely finding a surface that best-fits a data-set by minimising the sum of the square of the residuals [10]. The linear relationship of the parameters of a plane make this minimisation task easy, however, the more complex relationships in the equation of a sphere complicate the mathematics. The problem of fitting a sphere to a set of points in space is not one exclusive to metrology, but finds its place in archaeology, geography, and has been a topic of research since the early 60's [11].

Two popular least-squares approaches for the sphere-fit exist; the first relies on linearising the equation of a sphere (linear least-squares, LLS) and has been known since 1974 [12]. The second relies on an iterative approach, such as Gauss Newton, to find the minimum (non-linear least-squares, NLLS). Forbes [13,14] provides full details of the two approaches adopted for this study.

2.1. Summation least-squares

An alternative to these approaches for circle-fitting was identified by Bullock [15]; the mathematics are expanded here to a sphere-fit to supplement the former methods. This routine, referred to here as summation least-squares (SLS), makes use of domain shifting and substitution to simplify the equation of a sphere, resulting in a direct solution of a third-order simultaneous equation. This considerably reduces the computational cost when compared to the usual Jacobian matrix solver required by the alternatives.

Assume, a spherical surface of radius, r, comprising of n points at (x_i, y_i, z_i). The data can be translated into a new coordinate space (u, v, w) such that it has a new centre, (u_c, v_c, w_c), nominally the origin. With the centre as the origin, assumptions can be made about the distribution of the coordinates that allow the least-squares minimising function to be linearised.

Applying the following definitions:

$$\bar{x} = \frac{1}{n}\sum_{i=1}^{n} x_i, \quad \bar{y} = \frac{1}{n}\sum_{i=1}^{n} y_i, \quad \bar{z} = \frac{1}{n}\sum_{i=1}^{n} z_i, \tag{1}$$

and

$$u_i = x_i - \bar{x}, \quad v_i = y_i - \bar{y}, \quad w_i = z_i - \bar{z} \tag{2}$$

For a least-squares fit, we wish to minimise the function:

$$s = \sum_i g(u, v, w)^2 \tag{4}$$

where

$$g(u, v, w) = (u_i - u_c)^2 + (v_i - v_c)^2 + (w_i - w_c)^2 - \alpha \tag{5}$$

and

$$\alpha = r^2 \tag{6}$$

Following Bullock's approach, $S(u, v, w, \alpha)$ is partially differentiated with respect to u_c, v_c, and w_c to find the minima.

Using the following nomenclature:

$$\sum_i u_i = S_u, \quad \sum_i u_i^2 = S_{uu}, \quad \sum_i u_i^3 = S_{uuu}, \quad \sum_i u_i v_i = S_{uv}, \quad \text{etc.} \tag{7}$$

The partial derivatives are simplified to:

$$u_c S_{uu} + v_c S_{uv} + w_c S_{uw} = \frac{S_{uuu} + S_{uvv} + S_{uww}}{2} \tag{8}$$

$$u_c S_{uv} + v_c S_{vv} + w_c S_{vw} = \frac{S_{vuu} + S_{vvv} + S_{vww}}{2} \tag{9}$$

$$u_c S_{uw} + v_c S_{vw} + w_c S_{ww} = \frac{S_{wuu} + S_{wvv} + S_{www}}{2} \tag{10}$$

Eqs. (8)–(10) represent a third-order simultaneous equation, which can be written in the matrix form, $Ax = b$:

$$\begin{bmatrix} S_{uu} & S_{uv} & S_{uw} \\ S_{uv} & S_{vv} & S_{vw} \\ S_{uw} & S_{vw} & S_{ww} \end{bmatrix} \begin{bmatrix} u_c \\ v_c \\ w_c \end{bmatrix} = \frac{1}{2} \begin{bmatrix} S_{uuu} + S_{uvv} + S_{uww} \\ S_{uuv} + S_{vvv} + S_{vww} \\ S_{uuw} + S_{vvw} + S_{www} \end{bmatrix} \tag{11}$$

This is solved for u_c, v_c, w_c by pre-multiplying both sides by A^{-1}.

To find the radius, r:

$$\alpha = r^2 = u_c^2 + v_c^2 + w_c^2 + \frac{S_{uu} + S_{vv} + S_{ww}}{n} \tag{12}$$

And translating the centres back into (x, y, z) space:

$$x_c = u_c + \bar{x}, \quad y_c = v_c + \bar{y}, \quad z_c = w_c + \bar{z} \tag{13}$$

On evaluating the time taken to process 100,000 data-sets comprised of 51×51, 101×101 and 201×201 data points for LLS and SLS, both algorithms' timings scale approximately linearly with the number of data points. Furthermore, the SLS algorithm is approximately twice as fast as LLS.

3. Sources of measurement error

Looking at the elements of a raster-scanning, coordinate measurement machine, such as the XYRIS 4000, it is relatively straightforward to identify sources of potential error. These are categorised into two areas, motion system errors and sensor errors.

Motion system errors may include:

- Stage resolution and accuracy – the smallest measurable step and the relationship between theoretical and real-world position;
- Stage run-out – while at a nominally linear velocity during scanning, there is an acceleration and deceleration phase;
- Stage pitch and roll – despite using high-end motion stages, the sample will still wobble microscopically as it moves;
- Thermal expansion – both the metal stages and the granite gantry expand and contract with changes in temperature;
- Non-orthogonal axes – alignment of the three different motion systems that combine to raster scan the sample and adjust the height of the sensor.

Sensor errors may include:

- Abbe Error – the sensor is unlikely to be aimed perfectly perpendicular to the measurement stages;
- Linearity – the response of the probe does not follow the actual displacement;
- Spot size – the finite focal spot-size causes an averaging effect;
- Sensor noise – random ripple on the output, even in steady-state conditions;
- Thermal response – temperature effects on air density;
- Angular tolerance – the slope of the sample may be too high to return light;
- Gauge range – the range of surface heights over which the sensor will operate.

In addition to the above errors, there are also a number of parameters that the user configures at the start of the measurement, all

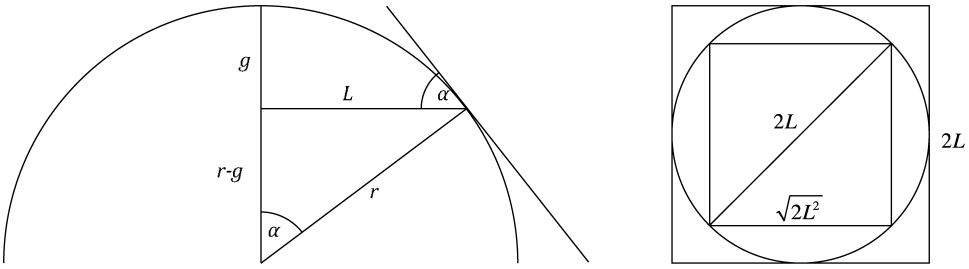

Fig. 1. Surface inclination angle and maximum measurable length of a sphere.

of which may impact the performance of the sphere-fitting; these are defined below:

- Number of data points in x and y – defines the grid spacing;
- Measurement length in x and y – defines the measurement area;
- Centre of measurement area – for spherical measurements this is typically the highest point or 'crown'.

The user influenced parameters defined above are varied in a designed experiment in order to both optimise the parameter settings for the measurement of spherical surfaces, and to investigate the influence of these parameters on the new method for comparison with the LLS and NLLS algorithms.

4. Designed experiment

For the purpose of this study, an ideal spherical surface of radius 22.00064 mm is used, the radius being that of a standard calibration sphere. Sun et al. [7] showed that increasing the number of data points from 21×21 to 51×51 decreased both the bias and uncertainty of radius estimation for a constant segment angle; in this study the number or data points is varied from 51×51 to 201×201.

When generating the ideal spherical surface, the sensor performance is considered; the XYRIS 4000 uses a confocal laser (CL) with a gauge range and angular tolerance of 0.6 mm and 17° respectively. If a square sampling area is adopted, and only the sensor gauge range is considered, the maximum measurable length $2L$ for the CL sensor is given by:

$$2L = 2\sqrt{g(2r - g)} \tag{14}$$

where r is the radius of the sphere, and g is the gauge range of the sensor; see Fig. 1.

From Fig. 1 it can be seen that the surface inclination angle α for a sphere is given by:

$$\alpha = \sin^{-1}\left(\frac{L}{r}\right) \tag{15}$$

Using (14) and (15), the maximum measurable length of a spherical surface can be calculated for a given sensor specification and sphere radius. In this case, the gauge range of 0.6 mm is the limiting factor giving a maximum measurement length of 10.206 mm. This measurement length results in a significant region being omitted as it falls out of gauge range and angular tolerance; see Fig. 2A and

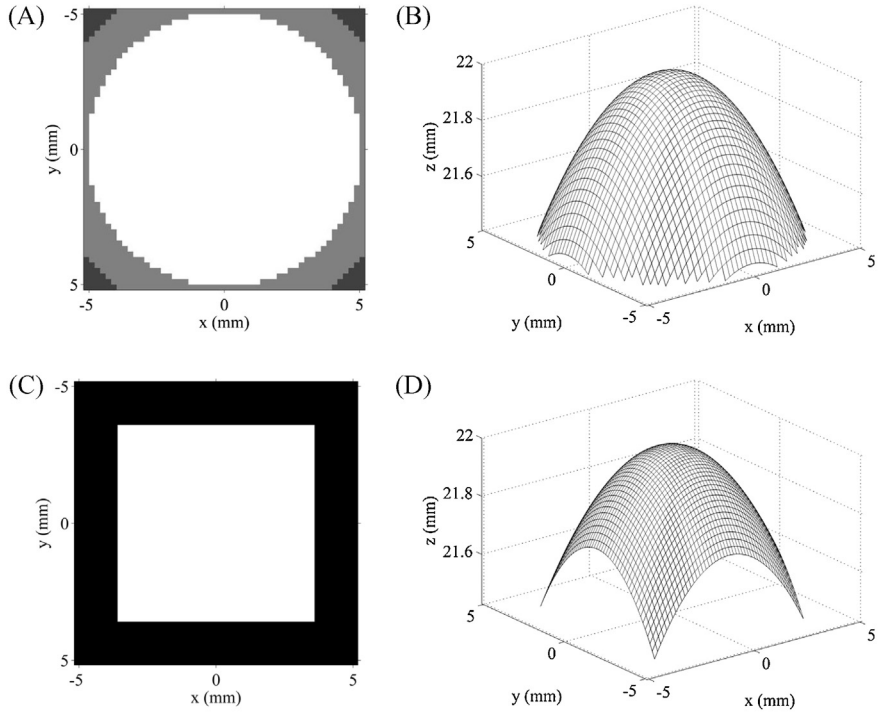

Fig. 2. Two measurement areas for spherical surfaces: white pixels are data in range, light grey pixels are data loss due to angular tol., dark grey pixels are data loss due to both gauge range and angular tol., black pixels are data outside the measurement area. (A) Data loss for $2L$ measurement length. (B) Ideal spherical surface for $2L$ measurement length. (C) Data loss for $\sqrt{2L^2}$ measurement length. (D) Ideal spherical surface for $\sqrt{2L^2}$ measurement length.

Table 1
Factors and their respective levels.

Factor	Level	
	1	2
(A) Data points	51 × 51	201 × 201
(B) Crown offset in *x*, *y* (μm)	0.0, 0.0	25, 25
(C) Measurement length (mm)	7.217	10.206

B. To minimise this drop-out, it is common practise to measure a square region inscribed by the circle with each side of length $\sqrt{2L^2}$, as shown in Fig. 1, however, by doing this a significant portion of the high segment angle data is excluded, as shown in Fig. 2C and D.

When measuring nominally spherical surfaces, the sample must first be 'crowned', where the highest point of the surface is determined and then repositioned as the centre of the measurement area. This maximises the measured area given the limitations of the gauge range and angular tolerance of the sensor. Crowning is often carried out by an auto-crown routine, the accuracy of which is limited to the resolution of the scan; consider a scan with 201 × 201 data points and a measurement length of 10 mm, the grid size would be 50 μm. It is reasonable to assume this error could be reduced by linear interpolation to half a grid spacing, *i.e.* ±25 μm.

The user defined parameters previously identified are hereafter referred to as factors and are presented in Table 1 alongside their respective factor levels; the response measured in this experiment is the absolute radius error. A three factor, two level, full factorial experiment is run for each of the three sphere-fitting algorithms. The experiment design and results are presented for each sphere-fitting algorithm in Table 2. To evaluate the impact of each factor, the average value of the response when the factor is at level 1 is compared with the average value of the response when the factor is at level 2; the difference measures the effect of the factor on the radius error. A negative effect indicates that changing from level 1 to 2 has a beneficial effect. All effects are summarised graphically in an effects plot, see Fig. 3.

4.1. Designed experiment results

As expected, increasing the number of data points has the effect of reducing the estimated radius error; see Fig. 3, factor A. While this observation should impact on user parameter selection, it is important to realise the difference between simulation and real-world measurements. Increasing the number of data points will increase the total measurement time, allowing effects such as thermal drift to degrade performance; more data points may therefore be in contradiction to good experimental set-up.

The effects plot suggests that by introducing a crown offset, the estimated radius error reduces; see Fig. 3, factor B. This observation is explained by looking to runs 7 and 5 in Table 2; these both represent 51 × 51 data points over the larger measurement area, with and without a crown offset respectively and show that the offset reduces the estimated radius error. To explain this result we must look to the range of *z*-values and the number of data points in range for runs 7 and 5, as shown in Table 3. Table 3 shows there is a larger range of *z*-values with a crown offset than without, also that there are more data points in range with a crown offset than without. This suggests that the 51 × 51 data point sampling is too coarse and valuable gauge range is lost with no crown offset. This calls for adaptive sampling [16], whereby the grid spacing becomes finer where the surface inclination angle becomes large or approaches the limit of the sensor's angular tolerance.

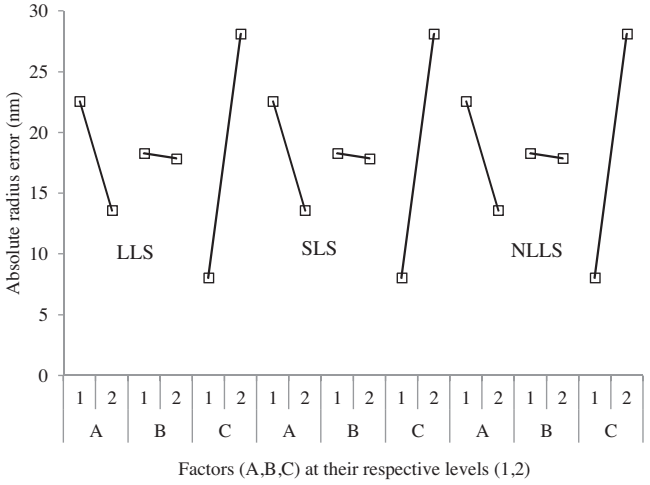

Fig. 3. Results of the designed experiment shown in the form of an effects plot.

Factor C dominates the effects plot, this being the measurement length; surprisingly the results suggest that the larger measurement area leads to a larger radius error. Table 3 shows that for the smaller measurement area (runs 1–4) more data points are in range; this is intuitive since the smaller scan area is chosen to maximise the number of points within the gauge range and angular tolerance of the sensor. The larger scan area increases the range of *z*-values captured; again the reason for its choice. It seems that when estimating the radius of a sphere, increasing the range of *z*-values has less significance than the number of data points in range. Therefore, the results of the designed experiment suggest using the $\sqrt{2L^2}$ measurement length.

5. Monte Carlo simulation of surface noise

In order to further assess and compare the performance of the three least-squares methods, a Monte Carlo simulation is conducted, whereby ideal spherical data is generated, then superimposed with varying degrees of surface irregularities and the radius evaluated by all three sphere-fitting algorithms.

Perfect spherical data is generated for both measurement lengths discussed in the previous section at 51 × 51 data points. Surface irregularity is simulated by adding zero mean, Gaussian

Table 2
Response table for all sphere-fitting algorithms.

Run	Factor			Absolute radius error (nm)		
	A	B	C	LLS	SLS	NLLS
1	1	1	1	5.68	5.68	5.69
2	2	1	1	4.06	4.06	4.05
3	1	2	1	16.09	16.09	16.10
4	2	2	1	6.35	6.35	6.36
5	1	1	2	41.81	41.81	41.80
6	2	1	2	21.63	21.64	21.63
7	1	2	2	26.68	26.69	26.68
8	2	2	2	22.36	22.36	22.35

Table 3
Data in-range for each run of the designed experiment.

Run	Range of *z*-values (mm)	Data points in range	Percentage of 'good' points
1	0.57616	2597	99.85
2	0.59395	40,397	99.99
3	0.59157	2598	99.88
4	0.59632	40,396	99.99
5	0.59221	1941	74.63
6	0.59982	31,397	77.71
7	0.59881	1961	75.39
8	0.59996	31,430	77.80

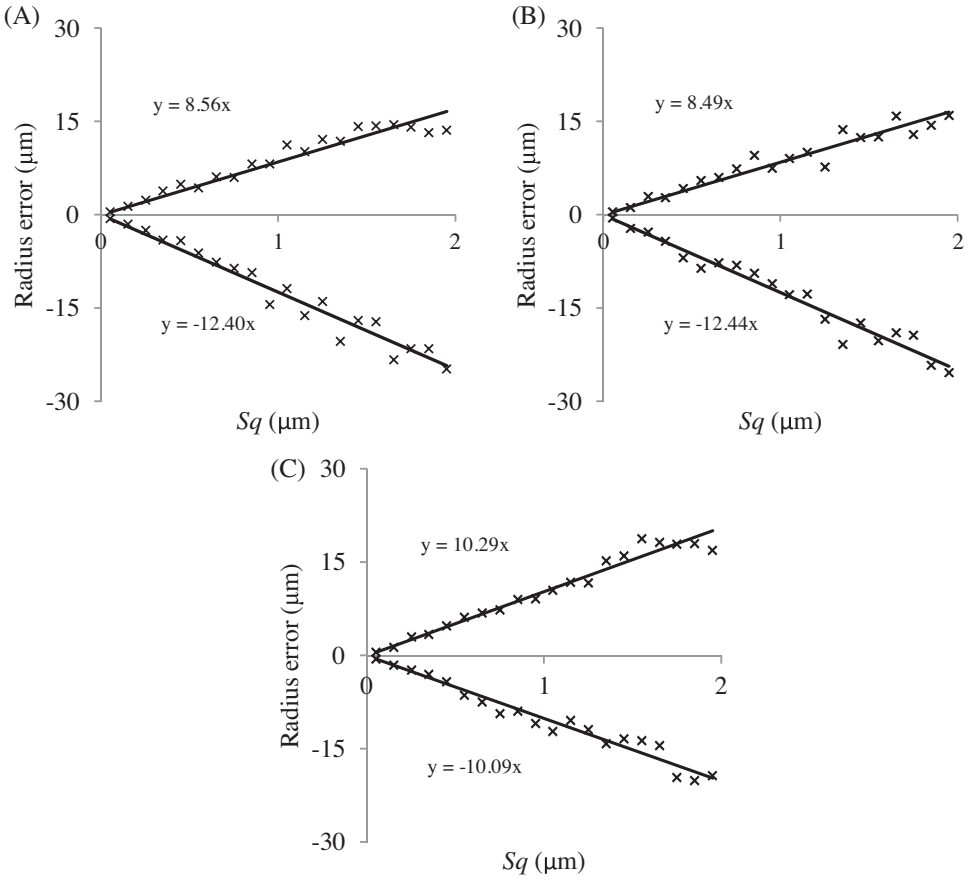

Fig. 4. Trend lines fitted to limits of radius error distribution from repeated simulations for 2*L* measurement length, evaluated by the (A) LLS algorithm, (B) SLS algorithm and (C) NLLS algorithm.

distributed noise to the *z*-dimension of the ideal surface; this considers both surface roughness, and random noise from the measurement system. The standard deviation of the noise is varied between 50 nm, this being the random noise from a con-focal white light sensor [5], and a higher limit of 2 µm. The noise is generated using a pseudorandom number generator in Matlab (MathWorks, MA, USA). It should be noted that the standard deviation of a zero mean, Gaussian distribution is mathematically equivalent to the RMS height, *Sq*, of the surface after sphere-fitting, as per ISO 25178-2 [17]. Therefore the *Sq* of the surface is varied over the previously stated range.

A Monte Carlo approach is adopted, whereby each noise waveform is first generated to a precision of 10 nm (the resolution of the sensor), then superimposed on the ideal spherical surface; the radius of the ideal surface with superimposed noise is then estimated using all three sphere-fitting algorithms; this is repeated 1000 times for each *Sq* value.

5.1. Monte Carlo simulation results

For each 1000 repeated simulations, the standard deviation, skewness and limits of the radius error distribution are evaluated. Fig. 4A–C shows, for the 2*L* measurement length, the limits of the radius error distribution plotted against *Sq* for each sphere-fitting algorithm. In each case trend lines are fitted to the data points and the gradients evaluated; Table 4 summarises the gradients of the trend lines for both the 2*L* and $\sqrt{2L^2}$ measurement lengths. When plotting the standard deviation of the radius error against *Sq* a linear relationship is seen, and fitting a trend line gives a gradient of 3.2 for all three sphere-fitting algorithms and for both measurement lengths.

Considering the gradients of the trend lines fitted to the limits of the radius error distribution for LLS and SLS in Fig. 4 and Table 4, it is clear that these algorithms closely follow each other; this similarity is most likely due to both routines linearising the equation of a sphere. Also, the gradients are mostly larger for the $\sqrt{2L^2}$ measurement length than the 2*L* measurement length; this result suggests

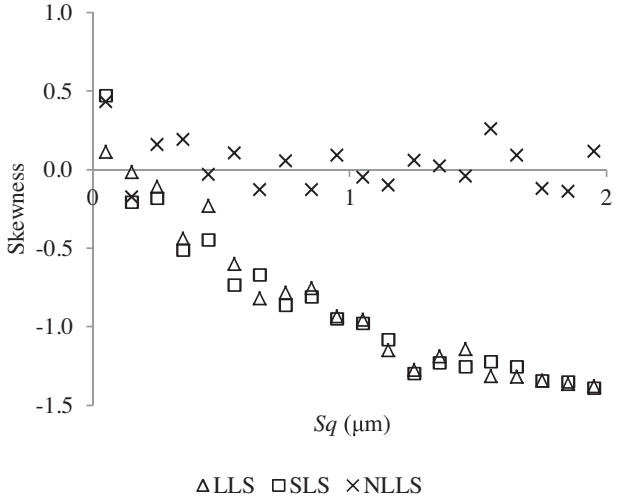

Fig. 5. Skewness of Monte Carlo results for a 22.00064 mm radius sphere, 2*L* measurement length.

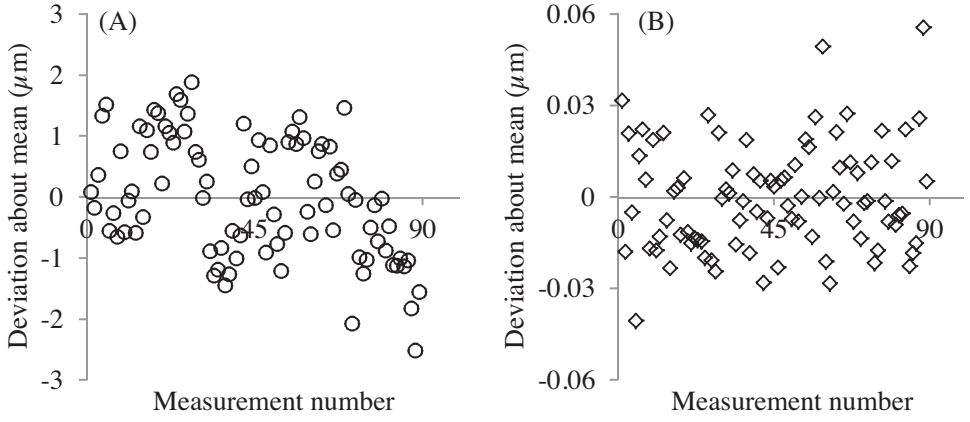

Fig. 6. (A) Deviation of radius about its mean value. (B) Deviation of *Sq* about its mean value.

that the larger range of *z*-values, achieved by the larger measurement length ($2L$), reduces the variation of radius estimates when compared to the smaller measurement length ($\sqrt{2L^2}$). Therefore, the $2L$ measurement length leads to more precise measurements, as per the Monte Carlo results, whilst the $\sqrt{2L^2}$ measurement length leads to more accurate measurements, as per the designed experiment results.

One further observation made from both Fig. 4 and Table 4 is that both SLS and LLS exhibit a clear bias, with a larger negative error limit gradient than positive error limit gradient; this suggests the radius error distribution is not symmetric about zero. Fig. 5 shows the results of plotting the skewness of each distribution for the $2L$ measurement length. The skewness of the NLLS algorithm is clearly grouped around the origin suggesting a symmetric distribution, while both LLS and SLS algorithms show an increasingly negative skewness as *Sq* increases. The Kurtosis plots have been omitted since all three algorithms showed a constant trend scattered around 3.0, *i.e.* a 'normal' distribution. The skewness of the linear algorithms suggests they tend to underestimate radius. On reviewing the literature, this radius underestimation has previously been acknowledged for linear circle-fitting algorithms [18,19]. Chernov and Lesort [20] state that the linear least-squares circle-fitting algorithm grossly underestimates radius for small circular arcs, thus this property should be expected when sphere-fitting to small segment angled spheres.

6. Uncertainty estimation

The plots in Fig. 4 allow an estimation of radius uncertainty for real-world measurements, provided the Monte Carlo simulation matches the measurement conditions in terms of sphere-fitting algorithm, nominal sphere radius, number of data points, and measurement length.

To demonstrate this method, a calibrated sphere of 22.00064 mm radius is measured 100 times on a XYRIS 4000 fitted with a CL sensor. The sample is crowned, the measurement length is set as 10.206 mm, and 51×51 data points are measured. The measured surfaces are processed using the NLLS sphere-fitting algorithm, and the remaining surface after sphere-fit, the residual, is evaluated for its *Sq*.

Fig. 6A and B shows the deviation of the radius and the *Sq* about their respective means for the repeat measurements. Fig. 6B shows the deviation of *Sq* is small in comparison to that of the radius, therefore only a few repeated measurements are required to estimate *Sq*; for this example the mean of the first seven repeats is used. With this estimate of *Sq*, alongside Fig. 4C, the limits of the radius error distribution are estimated: in this case *Sq* is 0.29 μm, which gives radius error limits of +2.98 and −2.93 μm. Using the larger limit for safety reasons, the radius uncertainty of the sphere-fitting algorithm for this measurement is estimated as ±2.98 μm. ISO 14253 part 2 [21] states two times the standard deviation is used as the limit of a Gaussian distribution: two times the standard deviation of the 100 radius measurements is equal to 1.95 μm, this appears to be a little conservative compared to the proposed method; however, three standard deviations shows good agreement at 2.93 μm. Hence the Monte Carlo method can be used to estimate the radius uncertainty instead of conducting a large number of repeated measurements and evaluating the standard deviation.

The radius uncertainty of the sphere-fitting algorithm is incorporated in an uncertainty budget as follows:

$$U = K\sqrt{u_{cal}^2 + u_{SF}^2 + u_T^2} \tag{16}$$

where u_{cal} is the radius uncertainty of the calibration sphere, as per the calibration certificate, and is equal to ±0.3 μm; u_{SF} is the uncertainty of the sphere-fitting algorithm, evaluated above as ±2.98 μm; u_T is the uncertainty due to the thermal expansion of the calibration sphere and is equal to 0.11 μm for an expansion coefficient of $4.9 \times 10^{-6}\,^{\circ}\mathrm{C}^{-1}$ and a change in temperature of ±1 °C; finally *K* is the coverage factor, and is equal to 2 for a confidence level of 95%. Therefore the expanded radius uncertainty is estimated as ±5.99 μm.

Table 4
Gradients of trend lines fitted to limits of radius error distribution for both measurement lengths and for all three sphere-fitting algorithms.

	LLS	SLS	NLLS
Pos. error gradient $2L$	8.56	8.49	10.29
Neg. error gradient $2L$	−12.40	−12.44	−10.09
Pos. error gradient $\sqrt{2L^2}$	8.88	8.53	10.84
Neg. error gradient $\sqrt{2L^2}$	−12.38	−12.73	−10.58

7. Conclusions

A recently proposed linear circle-fitting algorithm has been extended to a sphere-fitting algorithm and demonstrated to perform comparably to the long-standing LLS algorithm commonly used in metrology software; this match has been attributed to the linearisation of the sphere-fit equation used in both algorithms.

User defined scan parameters were varied in a designed experiment in order to both optimise parameter settings, and to investigate their influence on the accuracy of the SLS, LLS and NLLS algorithms. The results showed all three algorithms to have similar performances, and highlighted that coarse grid spacing can lead to data loss due to the sensor gauge range being exceeded, ultimately leading to an increase in radius error. The designed experiment also highlighted that a scan area chosen to maximise the number of points within the gauge range and angular tolerance of the sensor leads to more accurate radius estimates than increasing the range of *z*-values captured; achieved by using a larger scan area.

In order to further assess the performance of the three least-squares methods a Monte Carlo approach was adopted, whereby noise waveforms were generated then superimposed on an ideal spherical surface; the radius of the resulting surface was then estimated using all three sphere-fitting algorithms over a range of noise amplitudes. The results showed that the limits of the radius error distribution increased in an approximately linear fashion with increasing noise amplitude; also, the standard deviation of the radius error increased linearly with noise amplitude. While this was true for all three sphere-fitting algorithms, the radius error distribution was noticeably negative for the LLS and SLS algorithms; both linear algorithms showed an increasingly negative skewness as noise amplitude increased. Linear circle-fitting algorithms have previously been shown to underestimate radius, it follows that this holds for sphere-fitting.

Finally, the output of the Monte Carlo simulation has been presented as a method for estimating the radius measurement uncertainty. The method relates the *Sq* of the residual to the limits of a radius error distribution generated by simulating the measurement process. The proposed approach mitigates the need for a high number of repeated measurements, but rather only a few repeats are required to estimate the *Sq* of the residual.

Acknowledgement

The authors would like to thank Tom Bull of TaiCaan Technologies Ltd. for his assistance measuring the calibration sphere on the XYRIS 4000.

References

[1] Cross KJ. An investigation into the surface characteristics of three dimensional objects [Ph.D. thesis]. University of Southampton; 1996.
[2] McBride JW, Hill M, Loh J, Zhang D. Sensitivity of a 3-D surface mapping system to environmental perturbations. In: Laser metrology & machine performance V. Southampton, UK: WIT Press; 2001. p. 187–95.
[3] McBride JW, Cross KJ. The measurement and analysis of the three-dimensional form of curved surfaces. International Journal of Machine Tools and Manufacture 1996;36(5):597–610.
[4] Barakat NA, Elbestawi MA, Spence AD. Kinematic and geometric error compensation of a coordinate measuring machine. International Journal of Machine Tools and Manufacture 2000;40(6):833–50.
[5] McBride JW, Maul C. The 3D measurement and analysis of high precision surfaces using con-focal optical methods. IEICE Transactions on Electronics 2004;E87-C(8):1261–7.
[6] Loh J, McBride JW, Hill M, Zhang D. Analysis of linear and angular errors of a small coordinate measuring machine (SCMM). In: Sixth international conference on laser metrology, machine tool, CMM and robot performance. Southampton, UK: WIT Press; 2003. p. 245–55.
[7] Sun W, Hill M, McBride JW. An investigation of the robustness of the nonlinear least-squares sphere-fitting method to small segment angle surfaces. Precision Engineering 2008;32(1):55–62.
[8] Jung M, Cross KJ, McBride JW. A method for the selection of algorithms for form characterization of nominally spherical surfaces. Precision Engineering 2000;24(2):127–213.
[9] Zhang D. The assessment and application of form evaluation algorithms in coordinate metrology [Ph.D. thesis]. University of Southampton; 2003.
[10] Least-squares fitting; 2012. http://mathworld.wolfram.com/LeastSquaresFitting.html
[11] Robinson SM. Fitting spheres by the method of least squares. Communications of the ACM 1961;4(11):491.
[12] Kasa I. A curve fitting procedure and its error analysis. IEEE Transactions on Instrumentation and Measurement 1976;25(1):8–14.
[13] Forbes AB. Least-squares best-fit geometric elements. NPL Report DITC 140/89; 1991.
[14] Forbes AB. Robust circle and sphere fitting by least squares. NPL Report DITC 153/89; 1989.
[15] Bullock R. Least-squares circle-fit; 2006 http://www.dtcenter.org/met/users/docs/write_ups/circle_fit.pdf
[16] Wang J, Jiang X, Blunt L. Simulation of adaptive sampling in profile measurement for structured surfaces. In: Computing and engineering researchers conference. University of Huddersfield; 2010.
[17] ISO 25178-2. Geometrical product specifications (GPS) – surface texture: areal; 2012.
[18] Gander W, Golub GH, Strebel R. Least squares fitting of circles and ellipses. BIT Numerical Mathematics 1994;34(4):558–78.
[19] Chernov N, Ososkov GA. Effective algorithms for circle fitting. Computer Physics Communications 1984;33:329–33.
[20] Chernov. N, Lesort C. Least squares fitting of circles. Journal of Mathematical Imaging and Vision 2005;23:239–52.
[21] ISO 14253-2. Geometrical product specifications (GPS) – inspection by measurement of workpieces and measuring equipment; 2011.